

Solution-Deposited and Patternable Conductive Polymer Thin-Film Electrodes for Microbial Bioelectronics

Chia-Ping Tseng, Fangxin Liu, Xu Zhang, Po-Chun Huang, Ian Campbell, Yilin Li, Joshua T. Atkinson, Tanguy Terlier, Caroline M. Ajo-Franklin, Jonathan J. Silberg, and Rafael Verduzco*

Microbial bioelectronic devices integrate naturally occurring or synthetically engineered electroactive microbes with microelectronics. These devices have a broad range of potential applications, but engineering the biotic–abiotic interface for biocompatibility, adhesion, electron transfer, and maximum surface area remains a challenge. Prior approaches to interface modification lack simple processability, the ability to pattern the materials, and/or a significant enhancement in currents. Here, a novel conductive polymer coating that significantly enhances current densities relative to unmodified electrodes in microbial bioelectronics is reported. The coating is based on a blend of poly(3,4-ethylenedioxythiophene)-poly(styrenesulfonate) (PEDOT:PSS) crosslinked with poly(2-hydroxyethylacrylate) (PHEA) along with a thin polydopamine (PDA) layer for adhesion to an underlying indium tin oxide (ITO) electrode. When used as an interface layer with the current-producing bacterium *Shewanella oneidensis* MR-1, this material produces a 178-fold increase in the current density compared to unmodified electrodes, a current gain that is higher than previously reported thin-film 2D coatings and 3D conductive polymer coatings. The chemistry, morphology, and electronic properties of the coatings are characterized and the implementation of these coated electrodes for use in microbial fuel cells, multiplexed bioelectronic devices, and organic electrochemical transistor based microbial sensors are demonstrated. It is envisioned that this simple coating will advance the development of microbial bioelectronic devices.

applications, including energy harvesting,^[2] chemical production,^[3] water remediation,^[4] and sensing for health and environmental applications.^[5–7] Despite the wide range of complicated functionalities that different microbial bioelectronic devices possess, they all share similar aspects in their design and fabrication to empower the device operation. These key features include microbial biofilm formation, ion and electron transfer, and mass transport of nutrient and waste. When the microbes are introduced at the startup of the microbial bioelectronics, they often form biofilms on the electrode surface via physiochemical interactions.^[8] The microbes then generate protons and electrons as part of the current production which represents cell to material information flow that enables biosensing,^[7] biocomputing,^[9] and power generation.^[10,11] The microbial bioelectronic devices normally operate at defined potentials to facilitate electron transfer between the redox-active proteins on the microbes and the electrodes with different energy levels.^[12] To sustain the long-term operation of the microbial bioelectronics, the microbes need sufficient nutrient and

waste flow to maintain cell viability.^[8,13] Furthermore, due to the microbes' ability to self-generate and self-repair, microbial bioelectronics are often cheaper and more robust to operate under harsh environmental conditions for longer durations relative to using purified enzymes.^[14]

1. Introduction

Microbial bioelectronics are devices that integrate naturally occurring or synthetically engineered, electroactive microbes with microelectronics.^[1] These devices have a broad range of potential


C.-P. Tseng, F. Liu, P.-C. Huang, Y. Li, R. Verduzco
 Department of Chemical and Biomolecular Engineering
 Rice University
 Houston, TX 77005, USA
 E-mail: rafaely@rice.edu

X. Zhang, I. Campbell, C. M. Ajo-Franklin, J. J. Silberg
 Department of BioSciences
 Rice University
 Houston, TX 77005, USA

J. T. Atkinson
 Department of Physics and Astronomy
 University of Southern California
 Los Angeles, CA 90007, USA

T. Terlier
 SIMS Laboratory
 Shared Equipment Authority
 Rice University
 Houston, TX 77005, USA

R. Verduzco
 Department of Materials Science and NanoEngineering
 Rice University
 Houston, TX 77005, USA

 The ORCID identification number(s) for the author(s) of this article can be found under <https://doi.org/10.1002/adma.202109442>.

DOI: 10.1002/adma.202109442

A grand challenge for the field of microbial bioelectronics is interfacing electrodes with microbes. The interface should be biocompatible, stable, and, in the case where electron transfer occurs, electronically and ionically conductive.^[15] The material at the interface must not be toxic to the cells, and it must support microbial growth and the formation of dense layers of electroactive biofilms.^[1,16] This latter property can be very challenging to achieve as it is unclear what physiochemical properties of the abiotic interface are needed by the microbes to develop into a robust conductive biofilm. Furthermore, the stability of the interface holds important roles in protecting the electrodes from microbially-induced degradation and corrosion and preventing the delamination of the material while working under changing biases and high-salinity environmental conditions such as sea water.^[17] Additionally, the electronic and ionic conductivities of the interface are both critical to the current generation and current transfer as the microbial bioelectronics lose electron transfer if the counterions, especially protons, do not diffuse and migrate to the bulk electrolyte due to transport limitations.^[11]

Prior approaches to engineering the cell–material interface can generally be classified as either 3D or 2D interface materials, where the former involve a thick interface that microbes can penetrate and occupy and the latter a thin film between the microbes and the electrode.^[15,18] Examples of 3D interface layers include thick films of conductive polymers such as polypyrrole (PPy) or poly(3,4-ethylenedioxythiophene)-poly(styrenesulfonate) (PEDOT:PSS) that encapsulate electroactive microbes,^[19,20] carbon-based cloths, foam, and felt which enable colonization by microbes and transport of biomolecules,^[18,21] and conductive, porous scaffolds.^[22] Examples of 2D interface layers include thin films of metal oxides,^[23,24] conductive polymers,^[25] and redox-active materials.^[26,27] Innovations in electrode design for microbial bioelectronic systems have been covered in a number of prior reviews.^[1,15,18,28–31]

2D and 3D interface materials have been successful for monitoring the activities of electroactive microbes, but they vary widely in terms of their ability to simultaneously meet many of the existing design challenges. For example, the highest current densities to date have been achieved in thick, 3D conductive coating layers.^[22,32] Unfortunately, these materials can be challenging to implement and require multiple processing steps to

fabricate. In addition, the chemical reactions for the encapsulation of live microbes in 3D porous electrodes may be toxic and require delicate control for the condition of the reactions.^[20] Furthermore, 3D porous electrodes are generally not compatible with electrode patterning, which is of interest for depositing small numbers of microbes at selected addresses on a device. Conversely, many of the previously reported 2D coatings can be more easily patterned. However, they are not as effective at increasing the current density or improving microbial adhesion to a surface.^[18] Hence, there is a need for new interface layers for microbial bioelectronics that increase current densities and can be easily deposited and patterned.

Herein, we report a novel conductive polymer coating that is compatible with standard microfabrication processes and significantly enhances current densities relative to unmodified electrodes in microbial bioelectronic devices. Our coating is based on a blend of PEDOT:PSS crosslinked with poly(2-hydroxyethylacrylate) (PHEA) along with a thin polydopamine (PDA) layer for adhesion to an underlying ITO electrode. The coating is easily applied from solution and crosslinked by UV-irradiation to produce a thin and conformal conductive polymer coating. When used as an interface layer with *Shewanella oneidensis* MR-1, we measure an increase in the current density by a factor of 178 compared to unmodified electrodes, an improvement factor that is higher than previously reported thin-film 2D coatings and 3D conductive polymer coatings. We characterize the chemistry, morphology, and electronic properties of the coatings. We envision that this simple coating can help advance the development of microbial whole-cell bioelectronics by implementing these coated electrodes for use in microbial fuel cells (MFCs), multiplexed bioelectronic devices, and organic electrochemical transistor (OECT)-based microbial sensors.

2. Results and Discussions

2.1. Polydopamine and Reactive Monomer Produce Stable and Conductive Thin-Film Coatings

Our electrode coatings were based on PEDOT:PSS/PHEA and an adhesive PDA layer on top of ITO-coated glass (Figure 1,

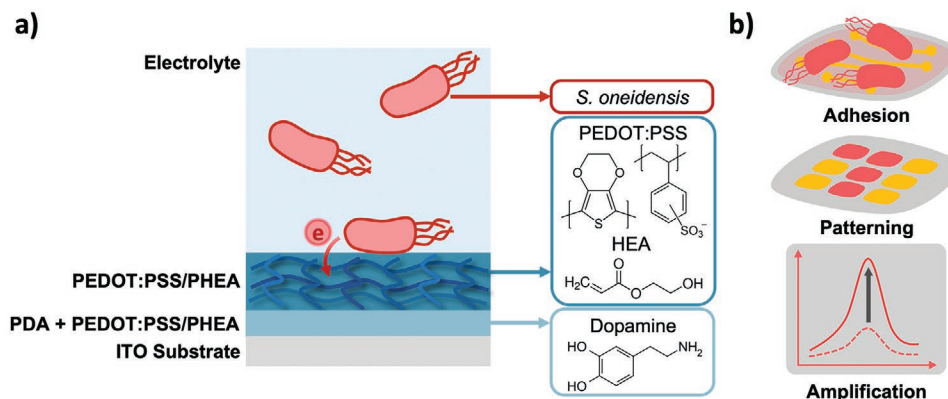


Figure 1. a) Schematic of the microbe–electrode interface showing the composition of the conductive PEDOT:PSS/PHEA coating on top of an adhesive PDA layer and ITO-coated glass substrate. These coatings were used to improve current fluxes when interfaced with *S. oneidensis*. b) These coatings serve to improve adhesion of electroactive microorganisms such as *S. oneidensis* and amplify electronic signals, and the films can be easily patterned on a surface.

Figure S1, Supporting Information). PEDOT:PSS is a commercially available conductive polymer dispersion used widely in organic electronic devices and applications.^[33–35] To produce stable coatings for long-term use in aqueous environments, we first coated the glass substrate with a thin (≈ 10 nm) layer of PDA using a previously reported method.^[36] Next, we added ethylene glycol (EG), 4-dodecylbenzenesulfonic acid (DBSA), and 2-hydroxyethyl acrylate (HEA) to create a liquid dispersion of PEDOT:PSS in water. EG and DBSA enhanced electronic conductivity and wettability of the film, while HEA served as a monomeric precursor for polyHEA (PHEA) which helped stabilize the film. The mixture was deposited on top of the PDA layer by spin-coating and exposed to 352 nm UV light for 2 h to polymerize the HEA and produce polyHEA (PHEA). The resulting film was stable in water and remained strongly adhered to the substrate even after immersion in water for up to 12 days. Both PHEA and PDA were necessary to produce stable film coatings. Without PHEA, the PEDOT:PSS coating fractured into small pieces after immersion in water for less than one day, and without PDA the film dewetted from the substrate surface during UV irradiation. Therefore, the combination of PEDOT:PSS/PHEA and PDA allows simple solution-processable coating of stable and conductive film on almost any kind of material while avoiding complex surface treatments including surface roughening,^[37] chemical modification,^[38] and nanomaterial incorporation.^[39]

We hypothesized that the PHEA stabilizes the film through hydrogen bonding interactions with the PEDOT:PSS, as has been reported in studies of similar materials.^[40] We performed Fourier-transform infrared spectroscopy (FTIR) to test this hypothesis. The FTIR spectra for HEA, PEDOT:PSS, and PEDOT:PSS/PHEA are shown in Figure S2, Supporting Information, and reveal both broadening and a large shift in the peak for O-H stretching for PEDOT:PSS/PHEA (3328 cm^{-1}) relative to HEA (3418 cm^{-1}). Furthermore, the O-H stretching peak is more intense in PEDOT:PSS/PHEA compared with PEDOT:PSS. These observations are consistent with our hypothesis that PHEA stabilizes the film due to hydrogen bonding interactions.

To characterize the chemical and physical properties of the electrode coatings, we used a combination of X-ray photoelectron spectroscopy (XPS), scanning electron microscopy (SEM), and atomic force microscopy (AFM). After deposition of the PDA layer, XPS measurements (Figure S3, Supporting Information) revealed a prominent peak at 400 eV, which corresponds to nitrogen core electron binding energy (N1s). After depositing the PEDOT:PSS/PHEA coating, the N1s peak disappeared and peaks at 230 and 165 eV corresponding to S2s and S2p binding energies were evident. This indicates that the PDA layer was uniformly coated with the PEDOT:PSS/PHEA film. Using SEM, we were able to visualize the top-down and cross-sectional images of the thin-film coating after cutting an edge of the film (Figure S4, Supporting Information). The SEM images revealed a uniform and thin-film coating. AFM measurements (Figure S5, Supporting Information) provided film thicknesses of 10 and 50 nm for the PDA and PEDOT:PSS/PHEA films. We performed additional AFM tapping mode experiments to compare the film morphologies of air-dried PEDOT:PSS, UV-cured PEDOT:PSS, air-dried PEDOT:PSS/HEA, and UV-cured

PEDOT:PSS/HEA, and the results of these experiments are shown in Figure S6, Supporting Information. There were no observable large morphological differences between these films. However, the images showed small decrease in roughness for the PEDOT:PSS/PHEA films after UV-curing, from 2.1 nm before curing to 1.9 nm after curing.

Additionally, we conducted time-of-flight secondary-ion mass spectrometry (ToF-SIMS) depth profiling experiments to examine potential mixing between PEDOT:PSS/PHEA and PDA (Figure S7, Supporting Information). Tracking the relative intensities for SO_3^- , CN^- , and InO^- ions reflected the relative compositions of PEDOT:PSS/PHEA, PDA, and ITO, respectively. The depth profile shows that the PEDOT:PSS/PHEA and PDA films are highly mixed near the bottom of the film at the interface with ITO, and the intensity for both decreases only near the ITO substrate. The significant infiltration of PEDOT:PSS/PHEA into the thin PDA coating can overcome the electrochemically inert properties of PDA and enable electron transfer from *S. oneidensis* to the ITO electrode via the PEDOT:PSS/PHEA coating.

2.2. Electrochemical Characterizations Show Low Resistance on Poly(3,4-ethylenedioxythiophene)-Poly(styrenesulfonate)/Poly(2-hydroxyethylacrylate) Coatings

In bioelectrochemical systems, the electrode materials should promote rapid charge transfer across the biotic–abiotic interface. To characterize the interfacial resistances and thin-film capacitances of the unmodified, PDA-coated, and PEDOT:PSS/PHEA-coated electrodes, we performed electrochemical impedance spectroscopy (EIS) (Figure 2). The EIS results were modelled with an equivalent circuit model (Figure S8, Supporting Information), enabling us to quantify the charge transfer resistance (R_{CT}), electrolyte resistance (R_{S}), and constant phase element impedance (CPE_{dl}). The estimated R_{CT} for unmodified, PDA-coated, and PEDOT:PSS/PHEA-coated electrodes in the abiotic systems were 2.0×10^5 , 1.3×10^5 , and $3497\ \Omega$, respectively, reflecting a large decrease in the charge-transfer resistance for the PEDOT:PSS/PHEA-coated electrodes. Furthermore, the capacitances for unmodified and PDA-coated electrodes were 2.7×10^{-5} and $3.5 \times 10^{-5}\text{ F}$, respectively, while that for PEDOT:PSS/PHEA-coated electrode was about three times larger at $1 \times 10^{-4}\text{ F}$. The Nyquist plot of the PEDOT:PSS/PHEA-coated electrode in the abiotic system displayed a characteristic semicircle indicating the charge transfer resistance. The charge transfer reaction is likely due to the electrochemical doping of the PEDOT:PSS/PHEA film. The conducting polymer PEDOT:PSS is initially at a polaronic (PEDOT^+) and/or neutral (PEDOT^0) state. When positive voltage is applied to the electrode, PEDOT^+ and PEDOT^0 are oxidized to bipolaronic (PEDOT^{2+}) and PEDOT^+ states and charge-compensating cations are expelled out of the PEDOT:PSS/PHEA film.^[41,42] The estimated R_{CT} for the unmodified, PDA-coated, and PEDOT:PSS/PHEA-coated ITO electrodes in the biotic systems were 1×10^5 , 0.9×10^5 , and $1325\ \Omega$. In both abiotic and biotic system, the R_{CT} for the unmodified and PDA-coated ITO electrodes are approximately the same and of the same order of magnitude. However, for the PEDOT:PSS/PHEA-coated ITO

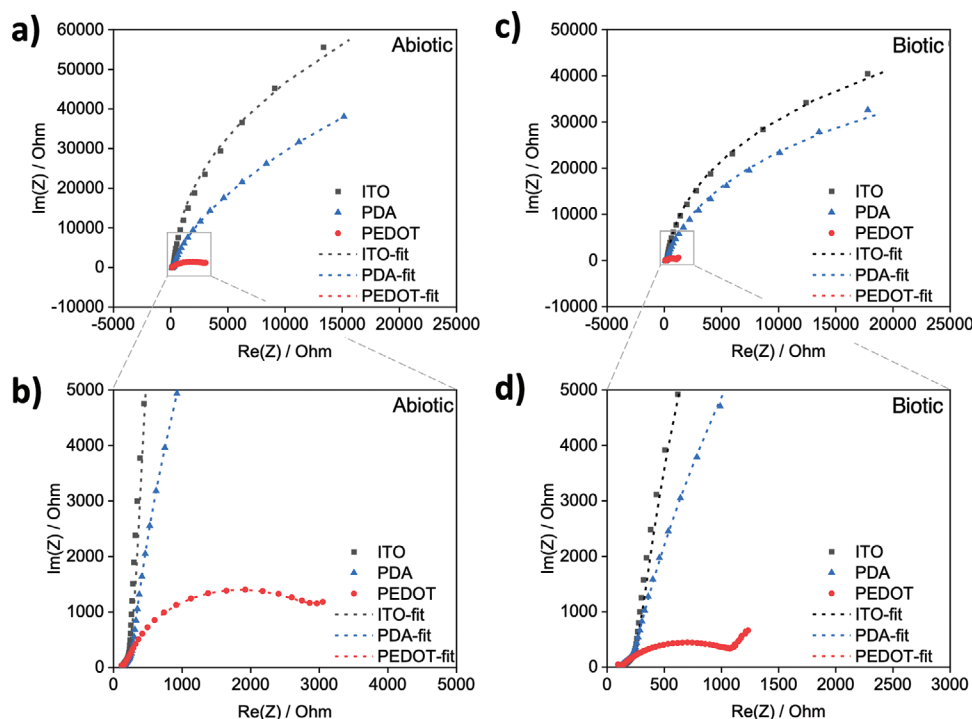


Figure 2. Characterization of interfacial impedance of fabricated electrodes using electrochemical impedance spectroscopy (EIS). a–d) Nyquist plots of unmodified, PDA-coated, and PEDOT:PSS/PHEA-coated electrodes in fresh SBM (a,b) and SBM inoculated with microbes for 25 h (c,d). These measurements demonstrate that the PEDOT:PSS/PHEA coatings reduce the resistance for interfacial charge transfer and resistance further decreases for PEDOT:PSS/PHEA coatings in the presence of microbes.

electrodes, the abiotic R_{CT} is more than twice as large as the biotic ones suggesting the improved electronic properties with the presence of microbes on the PEDOT:PSS/PHEA-coated ITO electrode, consistent with prior studies.^[13,43,44] Altogether, these results show that the PEDOT:PSS/PHEA-coated electrodes have a significantly lower R_{CT} and higher capacitance relative to the unmodified ITO and PDA-coated electrodes.

The electrode active surface area influences microbial adhesion and the number of contacting sites for interfacial charge transport.^[45] Ideally the electrodes should have a large interfacial area to maximize the cell–material interaction and signal with microbes. The active area of the electrodes was estimated by performing cyclic voltammetry with 10×10^{-3} M potassium ferricyanide in 1 M KCl solution. Redox behavior of ferricyanide ions was observed in both unmodified and PEDOT:PSS/PHEA-coated electrodes, while conversely no significant redox signals appeared for the PDA-coated electrodes, indicating that PDA-coated electrodes were not electrochemically active. The oxidation and reduction peak currents of the ferricyanide redox couple for the PEDOT:PSS/PHEA-coated electrodes were at similar magnitude when compared to the unmodified electrode (Figure S9, Supporting Information). Using the Randles–Sevcik equation (see Supporting Information),^[46,47] we estimated the active area of the PEDOT:PSS/PHEA-coated electrodes and the unmodified electrodes to be 0.38 and 0.40 cm², respectively, which represents a $\approx 5\%$ difference on the active area between the PEDOT:PSS/PHEA coating and the unmodified electrode. In sum, we see that the PEDOT:PSS/PHEA coating is smooth with its active area roughly the same as its unmodified counterpart.

2.3. Poly(3,4-ethylenedioxythiophene)-Poly(styrenesulfonate)/Poly(2-hydroxyethylacrylate) Coatings Enhance Microbial Adhesion, Viability, and Steady-State Current Densities in Microbial Whole-Cell Bioelectronic Devices

To study the impact of the thin-film coating on interfacial charge transport in a microbial whole-cell bioelectronic device, we tested three-electrode, single-chamber electrochemical reactors with either unmodified, PDA-coated, and PEDOT:PSS/PHEA-coated ITO electrodes with *S. oneidensis* MR-1 (Figure S10, Supporting Information). At the start of a measurement, the working electrode potential was poised at +0.2 V and the chamber was inoculated with a low density of *S. oneidensis* MR-1. The biotic current originating from microbial electron transfer was recorded continuously. As an abiotic control, we also conducted tests with the addition of media to the electrochemical reactor instead of *S. oneidensis* MR-1.

As expected, the abiotic negative control produced very low current densities of 4.6, 0.7, and 13.0 mA m⁻² for unmodified, PDA-coated, and PEDOT:PSS/PHEA-coated electrodes, respectively (Figure 3a and Figure S11, Supporting Information). This indicates that the lactate and growth medium do not generate significant currents and that the PDA-coated electrode was the least electrochemically reactive among all electrodes. When *S. oneidensis* MR-1 was added to the reactor, the current density increased significantly for both bare ITO and PEDOT:PSS/PHEA-coated electrodes, while the one for PDA-coated electrode only slightly increased (Figure 3b and Figure S11, Supporting Information). The current density had a steep increase and

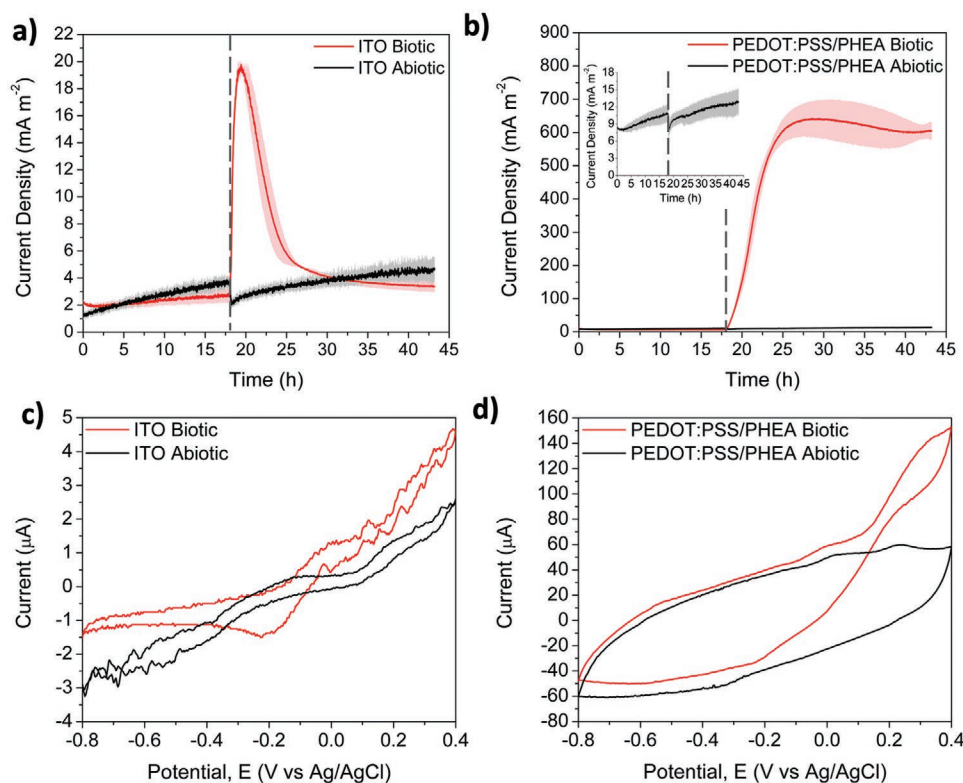


Figure 3. Electrochemical analysis of microbial whole-cell bioelectronic devices. a,b) Chronoamperometric measurements for biotic and abiotic electrochemical reactors with bare ITO glass (a) and PEDOT:PSS/PHEA-coated (b) working electrodes. The reactors were inoculated with *S. oneidensis* for biotic measurements marked with dashed line. Abiotic measurements contained medium. The working electrodes of the electrochemical reactors were poised at +0.2 V versus Ag/AgCl and 20×10^{-3} M of lactate was used as the carbon source for *S. oneidensis*. c,d) Cyclic voltammograms (scan rate: 10 mV s^{-1}) of biotic and abiotic samples on bare ITO glass (c) and PEDOT:PSS/PHEA-coated (d) electrodes after 43 h of chronoamperometric experiments.

reached a limited maximum of 19.8 mA m^{-2} within 2 h for the bare ITO electrodes but then sharply declined to a steady-state value of $\approx 3.4 \text{ mA m}^{-2}$ in less than 10 h. This steady-state current density was comparable to the current density measured in the abiotic reactors. The lowest current densities were measured for the PDA-coated electrodes. The biotic current measured with these electrodes reached a peak value of 1.2 mA m^{-2} , only slightly higher than the peak value (0.8 mA m^{-2}) measured under abiotic conditions. By comparison, the PEDOT:PSS/PHEA-coated electrodes reached peak current density of 642.6 mA m^{-2} 10 h after the inoculation, and the current densities maintained steady-state currents of 605.1 mA m^{-2} for up to 25 h after inoculation. The biotic current density was substantially greater than the abiotic current for the PEDOT:PSS/PHEA-coated electrodes, which indicated that this coating was effective in facilitating electron transfer from *S. oneidensis*. Comparing the PEDOT:PSS/PHEA-coated electrodes to the bare ITO electrode, the maximum and steady-state current densities increased by factors of 32 and 178, respectively. We attribute the distinct trends of the dynamic current densities for bare ITO and PEDOT:PSS/PHEA-coated electrodes to differences in the effectiveness of each surface supporting extracellular electron transfer (EET), cell growth, and metabolic activity. With the low density of the *S. oneidensis* MR-1 inoculated in the system, the initial increase in the current den-

sity for bare ITO electrode results from cells attaching to the electrode surface. Subsequently, the sharp drop of the current density indicates that the bare ITO electrodes cannot support continuous EET due to limited growth and metabolic activity of the cells on the surface. In contrast, the PEDOT:PSS/PHEA-coated electrodes exhibit a larger increase of the current density due to exponential cell growth on the surface followed by a plateau in the current density reflective of a stationary phase of cell growth with EET supporting the metabolic activity. Taken together, the chronoamperometric measurements confirm that the PEDOT:PSS/PHEA coatings effectively support the EET from microbes to the electrodes and can significantly enhance the current density.

S. oneidensis MR-1 can perform EET by delivering electrons from the cells to external electron acceptors using two different mechanisms. One mechanism is direct electron transfer (DET) in which outer membrane cytochrome serve as electron donors, while the other is the mediated electron transfer where electrons are shuttled from cells to materials by secreted mediators including flavins and quinones.^[48] These electron carriers hold distinct, characteristic midpoint potentials. To further understand the EET mechanism in the bioelectrochemical reactors, we conducted cyclic voltammetry measurements 25 h following the inoculation. Cyclic voltammetry was performed by sweeping the potential within the window of

−0.8 to +0.4 V for three cycles. The turnover cyclic voltammetry (CV) measurements of the biotic PEDOT:PSS/PHEA-coated electrodes produced higher current densities when compared with the unmodified and PDA-coated electrodes (Figure 3c,d and Figure S12, Supporting Information), consistent with the chronoamperometric data for these materials. Furthermore, the initiation of the catalytic wave was at −90 mV for biotic samples. It is known that the initiation of catalytic waves for cytochrome, ACNQ (2-amino-3-carboxy-1,4-naphthoquinone), and flavins are at ≈0, −300, and −500 mV, respectively.^[49,50] Our observed catalytic wave is most consistent with the outer membrane cytochrome, which is a major mechanism *S. oneidensis* MR-1 uses to transfer electrons to an electrode.^[50,51] This data suggests that the PEDOT:PSS/PHEA can accept electrons from cytochromes, which are one of the most widespread electron carriers in bioelectrochemical systems used for biosensing,^[7] biocomputing,^[52] and power generation.^[53]

The variation in current dynamics with surface modification suggested that the different electrode materials had different effects on the ability of *S. oneidensis* to conserve energy, grow, and remain viable on the electrode surface. To determine the impact of electrode material on cell viability, we used confocal microscopy to quantify the densities of live cells on the bare ITO glass and PEDOT:PSS/PHEA-coated electrodes. After 25 h of chronoamperometric measurements, cells were stained with SYTO 9 and propidium iodide (PI), and the live cell densities were estimated by counting the numbers of live and dead cells. We observed a clear difference in the density of microbes on the surfaces. On the unmodified electrodes, *S. oneidensis* attached to the electrode surface sparsely and evenly with the live cell density of $1.5 \pm 0.5 (\times 10^6)$ per cm^2 (Figure 4a). In contrast, the PEDOT:PSS/PHEA-coated electrode was densely covered with microbes with an estimated live cell density of $4.0 \pm 0.8 (\times 10^7)$ per cm^2 which was an order magnitude larger than the unmodified electrodes (Figure 4b). Green fluorescence was observed

on most microbes attached to the electrode surfaces and the ratios of the live/dead cells were estimated as 43.5 and 268.3 for unmodified and PEDOT:PSS/PHEA-coated electrodes, respectively. Thus, confocal microscopy reveals that PEDOT:PSS/PHEA-coated electrodes support excellent viability of microbes at the cell–material interface, and chronoamperometry indicates the effective electron transfer across the biotic–abiotic interface to allow cells to conserve energy and grow.

To study the surface morphology and microbial attachment, electrodes were also imaged using SEM. SEM images of the bare ITO glass electrode revealed a sparse distribution of microbes on electrode surface while the PEDOT:PSS/PHEA-coated electrodes exhibited a higher density of microbes, consistent with the confocal microscopy measurements (Figure 4c,d). Additionally, SEM images revealed regions of the PEDOT:PSS/PHEA-coated electrode surface that contained thick layers of microbes growing on the surface compared with a sparse monolayer observed on the bare ITO glass. These findings are consistent with prior reports that have found that ITO-coated glass is not a good surface for biofilm growth,^[54] but it is effective for microbial attachment.^[20,55]

Our results show that PEDOT:PSS/PHEA coatings improve the adhesion and viability of *S. oneidensis* on the electrode surface and enhance the charge transfer. We calculated the current output per cell by dividing the steady-state current density by the living cell density and obtained values of $\approx 200 \text{ fA cell}^{-1}$ ($1.2 \times 10^6 \text{ electron s}^{-1}$) and $\approx 1500 \text{ fA cell}^{-1}$ ($9.4 \times 10^6 \text{ electron s}^{-1}$) for bare ITO glass and PEDOT:PSS/PHEA-coated electrodes, respectively. This shows that the current enhancement is due to both greater attachment of microorganisms and a greater current output per live cell for the PEDOT:PSS/PHEA-coated electrodes. Predominantly, the low charge transfer resistance for the PEDOT:PSS/PHEA-coated electrodes decreases the resistance for electron transfer barrier and produces a larger current density compared to bare ITO electrodes. Furthermore,

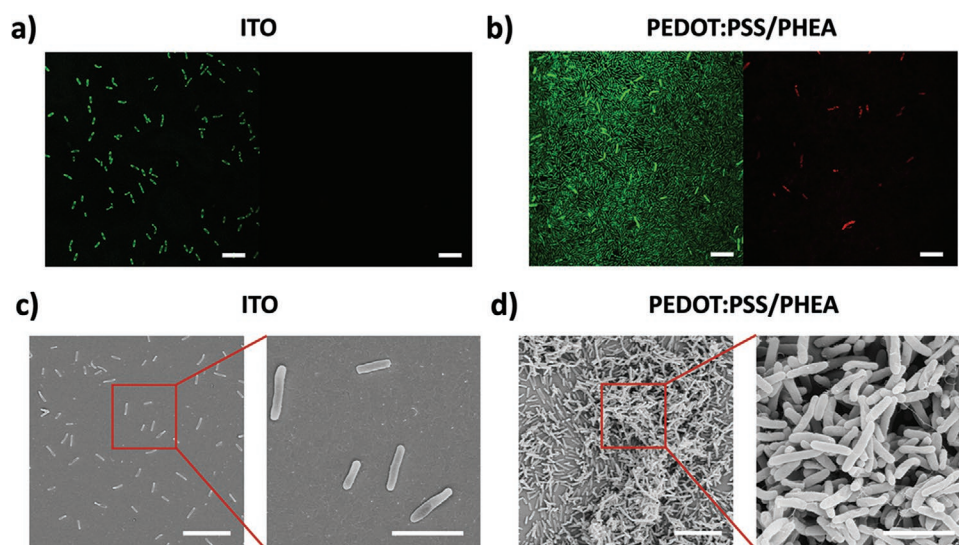


Figure 4. a,b) Confocal laser scanning microscopy images of bare ITO glass (a) and PEDOT:PSS/PHEA-coated (b) electrodes after 25 h of chronoamperometric current collection. The samples were stained with live/dead staining kit using SYTO 9 (green, live cells) and PI (red, dead cells). (Scale bar: 10 μm). c,d) SEM images of bare ITO glass (c) and PEDOT:PSS/PHEA-coated (d) electrodes after 25 h of chronoamperometric current collection. The samples were sputtered with 3 nm of Au prior to analysis. (scale bar: 10 μm for left images and 3 μm for right images enlarged from the left images)

the hydrated surface of the PEDOT:PSS/PHEA-coated electrodes likely increased the mass transport of nutrients from the medium when compared to the solid bare ITO electrodes. This improvement renders higher metabolic activity and enhances the output current density from EET per cell.^[44] Additionally, the mechanical properties of PEDOT:PSS/PHEA coatings are more compatible with microbes compared with unmodified ITO electrodes, and the coatings can conformally and seamlessly attach to the electrode surface for enhanced contact area and contact sites for DET.

The current density improvement for the PEDOT:PSS/PHEA-coated electrode is among the highest reported for microbial electrochemical systems (MESs). Representative examples of 2D and 3D electrode interface layers designed to increase current densities are listed in Table 1.^[56–67] Although 2D electrode interface layers in MESs usually generate lower absolute biotic current density compared with their 3D counterparts, we found that the improvement of current density using our PEDOT:PSS/PHEA-coated electrode surpassed that of other 2D and 3D interfaces. For example, a 2018 study reported that the steady-state current density increased a factor of 20 using a PEDOT:PSS-based, multilayer biocomposite interface layer.^[20] Another recent study used conductive polyelectrolytes to produce 3D bioelectrochemical composite layers which improved the current density by a factor of 150; at the time, this was the highest reported.^[43] While the absolute magnitude of the current density in our devices is lower than that for some previously reported microbial bioelectronic devices, the steady-state current output from our coated electrodes is large enough for use in many microbial bioelectronic applications, including

biosensors and power sources in which the minimum required current density is $\approx 0.01 \text{ A m}^{-2}$.^[68]

2.4. Poly(3,4-ethylenedioxythiophene)-Poly(styrenesulfonate)/Poly(2-hydroxyethylacrylate) Films Can Be Used for Power Generation and Sensing

Lastly, we investigated the use of PEDOT:PSS/PHEA-coated electrodes in microbial bioelectronic devices for power generation and sensing. First, we demonstrated that these electrodes could be used as part of a MFC to provide power to a light-emitting diode (LED) (Figure 5a). The electrochemical reactors were connected in series to produce a sufficient voltage to power a red LED (1.8 V). Each reactor provided an average voltage of $602.8 \pm 28.9 \text{ mV}$, and we were able to turn the LED on by connecting three electrochemical cells in series (Figure S13a, Supporting Information). This demonstrates that the processability of these coatings enable integration with low-power devices such as compact, microbial sensors.

Patterning of the electrodes for biosensing enables multiplexed detection of various electronic, ionic, or molecular signals in parallel. We explored the development of a proof-of-principle patterned electrode surface capable of interfacing with different strains of *S. oneidensis* MR-1 on a single substrate (Figure 5b). By patterning the electrode surface and applying a voltage only to selected regions of the electrode surface, we could selectively deposit fluorescent *S. oneidensis* MR-1 (GFP-expressing) and non-fluorescent *S. oneidensis* MR-1 on different regions of the surface. The patterned PEDOT:PSS/PHEA-coated

Table 1. Representative microbial electrochemical systems' anode modification and their performances in biotic current density improvement.

Dimension	Modification strategy	Anode materials	Microorganisms	Current enhancement factor ^{a)}
2D	PEDOT:PSS/PHEA thin film (this work)	ITO	<i>S. oneidensis</i> MR-1	178x
	rGO/Ag nanoparticles deposition ^{b)[57]}	Carbon paper	<i>S. oneidensis</i> MR-1	11.3x
	MWCNT coating ^{b)[58]}	Glassy carbon electrode	<i>S. oneidensis</i> MR-1	82x
	PEDOT electropolymerization ^[25]	Carbon paper	<i>S. loihica</i> PV-4	6x
	Iron (III) oxide nanocolloids precipitation ^[59]	ITO	<i>S. loihica</i> PV-4	80x
	Mixture of AC, NMP, and PVDF coating ^{b)[60]}	Graphite	Wastewater	1.3x
	CNT-textile composite ^[61]	Textile cloth	Wastewater	2.6x
	CNT/chitosan-nanocomposite coating ^[62]	Carbon paper	Wastewater	1.7x
	PEDOT:PSS electropolymerization ^[20]	Carbon felt	<i>S. oneidensis</i> MR-1	20x
3D	CPE-K polymer biomatrix blending ^{b)[43]}	Au electrode	<i>S. oneidensis</i> MR-1	150x
	PPy chemical polymerization ^[19]	Carbon cloth	<i>S. oneidensis</i> MR-1	4.8x
	GO aggregated and self-assembled ^{b)[63]}	Carbon cloth	<i>S. oneidensis</i> MR-1	25x
	PANI chemical polymerization ^{b)[64]}	Graphene foam	<i>S. oneidensis</i> MR-1	9x
	Gold nanoparticles precipitation ^[65]	Carbon plate	<i>G. sulfurreducens</i>	1.4x
	Inverse opal-indium tin oxide ^[22]	ITO	<i>G. sulfurreducens</i>	15x
	CPE-K loaded into biofilm ^[66]	Graphite plate	<i>G. sulfurreducens</i>	2.1x
	Freestanding graphene foam ^[32]	Graphene foam	<i>Geobacter</i> enriched culture	7x
	PVA-co-PE nanofibers spray-coating ^{b)[67]}	PPy/PET textile ^{b)}	<i>E. coli</i> K12	7x

^{a)}The current enhancement factor represents the ratio of the current for modified to unmodified electrodes for each modification strategy presented; ^{b)}GO: graphene oxide, MWCNT: multi-wall carbon nanotube, AC: activated carbon, NMP: N-methyl-2-pyrrolidone, PVDF: poly(vinylidene fluoride), CPE-K: polyelectrolyte, PANI: polyaniline, PVA-co-PE: poly(vinyl alcohol-co-polyethylene), PET: poly(ethylene terephthalate).

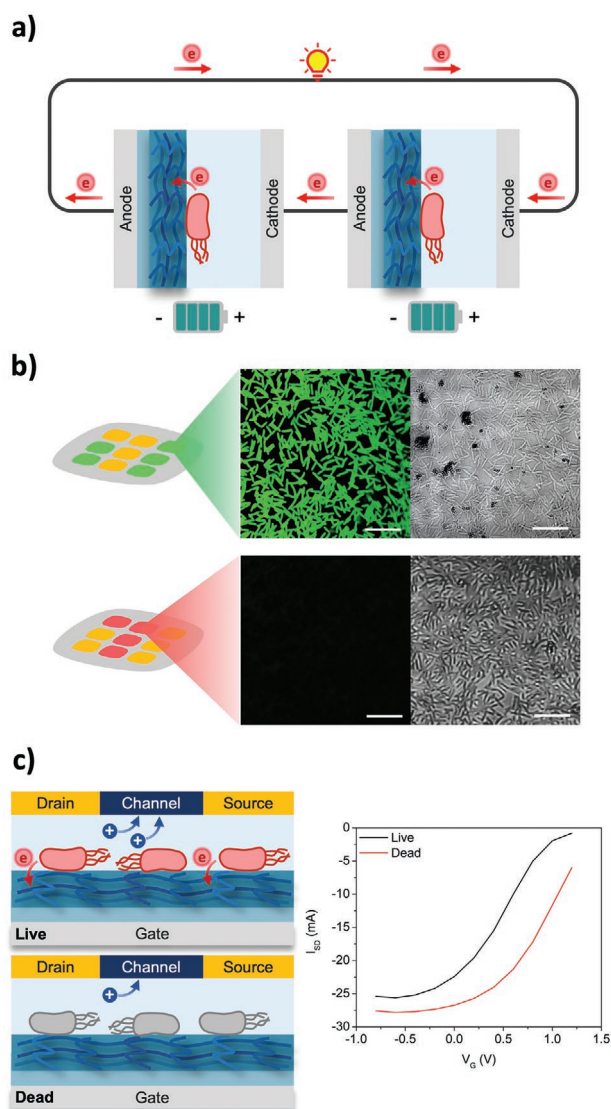


Figure 5. a) Schematic of microbial fuel cells connected in series to power red LED light. b) Confocal laser scanning microscopy images of PEDOT:PSS/PHEA-coated electrode deposited by *S. oneidensis* MR-1 with and without GFP (top: +GFP, bottom: -GFP). (scale bar: 10 μm) c) Schematics of the OECTs with the attachment of live and dead *S. oneidensis* on the PEDOT:PSS/PHEA-coated gate electrode and the response of I_{DS} before and after the cell-kill heating process.

electrode was fabricated using a simple plasma etching process and a poly(dimethylsiloxane) (PDMS) mask, and the patterned electrode consisted of two distinct and separately electronically addressable electrode regions (Figure S13b, Supporting Information). We first deposited GFP-labelled *S. oneidensis* MR-1 by introducing this strain to the electrochemical reactor and applying a potential of +0.2 V versus Ag/AgCl to one electrode region. Next, we exchanged the medium and introduced a non-labelled *S. oneidensis* MR-1 while applying a potential of +0.2 V versus Ag/AgCl to the other electrode region. Using bright field and confocal microscopy, we confirmed the presence of microbes on both electrodes, but only one electrode region was covered with fluorescently labelled *S. oneidensis* MR-1. This is

the first example to demonstrate the deposition of two different microbial strains at distinct regions on the same substrate. Our approach takes advantage of insoluble electron acceptor taxis^[67] or the electromigration of *S. oneidensis* toward the positive electrode during deposition.^[69] By applying a positive potential and introducing a specific strain of *S. oneidensis*, we can deposit the microbes only on a desired region of the electrode surface. Existing approaches for microbial patterning have primarily focused on using synthetic biology to engineer microbes to covalently attach to the electrode surface, for example, integrating gold-binding peptides or using heterologous pili.^[70–72] These approaches may only be applied to certain electrode materials or specific engineered microbes. The patterning technique developed herein will be useful for depositing multiple strains of engineered electroactive microbes at different addresses on the same device. Our method is straightforward to implement, and by depositing strains engineered to regulate EET using different analytes at different addresses, such devices should enable the parallel detection of various biomolecules.

Finally, we investigated the use of PEDOT:PSS/PHEA-coated electrodes in an OECT as a method to amplify electronic signals. OECTs are thin-film organic electronic devices that can amplify electronic, ionic, and molecular signals, and they have been implemented as chemical and biological sensors,^[73] including to interface with electroactive microbes.^[74] We designed and tested live and dead microbes on OECT devices. We deposited *S. oneidensis* MR-1 on a PEDOT:PSS/PHEA-coated gate electrode, and measured a transfer curve for the device (Figure 5c and Figure S14, Supporting Information). The transfer curve exhibited the expected decrease in current magnitude with increasing gate voltage, due to de-doping of the PEDOT:PSS channel. Next, we heated the gate electrode in medium at 70 °C for an hour to inactivate and kill the microbes and then repeated the transfer curve measurement. We observed a measurable shift in the current, as high as 5 mA. We attribute this shift in the transfer curve to the loss of DET from the microbe to the gate electrode, which serves to increase the effective voltage of the gate and de-dope the channel.^[74] This result demonstrates how a PEDOT:PSS/PHEA coating can be used as part of an OECT sensor to detect and amplify EET from microbes immobilized on the gate electrode. This design provides a potential route to microbial biosensors engineered to respond to specific targets by EET and to significantly amplify signals from one or few microbes.^[75]

3. Conclusions

We have developed a novel conductive polymer coating for microbial whole-cell bioelectronic devices. The coating was stable and could be easily deposited, crosslinked, and patterned, and when used in microbial bioreactors the coating produced a 178-fold increase in the steady-state current density relative to unmodified electrodes, the highest reported in literature. This enhancement in current density was attributed to a variety of factors: a higher density of microbes adhered to the modified electrodes, decreased charge transfer resistance and increased capacitance at the interfaces, and a larger contact area with microbes. We demonstrated that this coating can be used for

a variety of bioelectronic applications, including MFCs, multiplexed microbial devices, and OECTs. We envision that this simple coating will help advance the development of miniature, microbial whole-cell bioelectronic devices for applications as diverse as energy harvesting, chemical production, water remediation, and sensing for health and environmental applications.

4. Experimental Section

Materials: PEDOT:PSS Clevis PH1000 solution was purchased from Heraeus and used as received. ITO coated glass with sheet resistance of $20 \Omega \text{ sq}^{-1}$ was purchased from Kintec. All other chemicals were acquired commercially and used as received unless otherwise mentioned.

Electrode Fabrication: The electrode coating was prepared by deposition of a liquid dispersion of PEDOT:PSS with ethylene glycol (EG), 4-dodecylbenzenesulfonic acid (DBSA), monomer 2-hydroxyethylacrylate (HEA), and photoinitiator Irgacure 2959 on top of ITO-coated glass substrates. First, EG and DBSA were added to the commercial Clevis PH 1000 aqueous dispersion to final solution concentrations of 50 and $0.5 \mu\text{L mL}^{-1}$, respectively. Next, HEA (5 wt%) and photoinitiator Irgacure 2959 (0.1 wt%) were added to the dispersion, and the mixture was sonicated for 1 h. The solution was set aside while preparing the ITO-coated glass substrates.

ITO-coated glass was washed by sonication in soap water, deionized (DI) water, acetone, and isopropyl alcohol sequentially for 15 min each. The ITO was then blown dry using nitrogen gas and placed in petri dish for PDA coating. The PDA coating process was conducted following a previously reported protocol.^[76] In short, dopamine-HCl was dissolved in 1 M tris-HCl buffer to a final concentration of 2 mg mL^{-1} and buffered to pH 8.5. The ITO electrodes were then immersed in dopamine-HCl solution for 24 h at room temperature, producing a uniform PDA coating on the surface. Next, the surface of the electrodes was washed with DI water, and the PDA-coated ITO electrodes were blown dry using nitrogen gas. The electrodes were then immediately coated with PEDOT:PSS/HEA by spin-coating the PEDOT:PSS/HEA liquid dispersion at 300 rpm with an acceleration rate of 100 rpm s^{-1} for 30 s. The electrodes were then exposed to UV light (352 nm) for 2 h to crosslink the film. The as-fabricated electrodes were directly used in electrochemical experiments.

Electrode Patterning: The electrodes were patterned by exposing regions of the film to Fischione plasma cleaner 1020 and protecting regions of the coating with PDMS masks. The plasma cleaner is a high-frequency oscillating field system which is directly coupled to a quartz plasma chamber operated at 40 W. To prepare PDMS masks, the elastomer base was mixed with the curing agent in a 10:1 weight ratio. The mixture was vacuumed for 1 h to remove bubbles and then was polymerized under 80°C oven for 2 h, and the PDMS was cut into strips of $0.5 \text{ cm} \times 2.5 \text{ cm}$. The fabricated PEDOT:PSS/PHEA-coated electrodes were patterned by placing PDMS strips on the electrode to protect portions of the coating and applying plasma cleaning for 20 min with a mixture gas of 75% Ar and 25% O_2 to remove exposed regions of the surface.

Strains and Growth Conditions: *S. oneidensis* MR-1 was transformed with empty vector or a plasmid bearing green fluorescence protein (GFP),^[77] both harboring kanamycin resistant markers. Strains were cultured with *Shewanella* basal medium (SBM) containing $8.6 \times 10^{-3} \text{ M}$ NH_4Cl , $1.3 \times 10^{-3} \text{ M}$ K_2HPO_4 , $1.65 \times 10^{-3} \text{ M}$ KH_2PO_4 , $475 \times 10^{-6} \text{ M}$ $\text{MgSO}_4 \cdot 7\text{H}_2\text{O}$, $1.7 \times 10^{-3} \text{ M}$ $(\text{NH}_4)_2\text{SO}_4$, $100 \times 10^{-3} \text{ M}$ 4-(2-hydroxyethyl)-1-piperazineethanesulfonic acid (HEPES), 1x mineral mix (nitrilotriacetic acid (1.5 g), $\text{MnCl}_2 \cdot 4\text{H}_2\text{O}$ (0.1 g), $\text{FeSO}_4 \cdot 7\text{H}_2\text{O}$ (0.3 g), $\text{CoCl}_2 \cdot 6\text{H}_2\text{O}$ (0.17 g), ZnCl_2 (0.1 g), $\text{CuSO}_4 \cdot 5\text{H}_2\text{O}$ (0.04 g), $\text{AlK}(\text{SO}_4)_2 \cdot 12\text{H}_2\text{O}$ (5 mg), H_3BO_3 (5 mg), Na_2MoO_4 (0.09 g), NiCl_2 (anhydrous) (0.12 g), $\text{NaWO}_4 \cdot 2\text{H}_2\text{O}$ (0.02 g), and Na_2SeO_4 (0.1 g) per liter), and 1x vitamin mix (biotin (2 mg), folic acid (2 mg), pyridoxine HCl (0.02 g), thiamine (5 mg), nicotinic acid (5 mg), pantothenic acid (5 mg), cyanocobalamin (B-12) (0.1 mg), p-aminobenzoic acid (5 mg), and thiocetic acid (5 mg)

per liter), pH 7.2 supplemented with 0.05% (w/v) casamino acids, $20 \times 10^{-3} \text{ M}$ lactate, $50 \mu\text{g mL}^{-1}$ of kanamycin.^[78] Cultures were inoculated from glycerol stocks into 150 mL of Erlenmeyer flasks containing 50 mL of SBM and grown overnight at 30°C with shaking at 250 rpm. After incubation overnight, the cells were harvested by centrifugation at 4000 g for 10 min, washed, and resuspended in fresh SBM to a final OD600 of 1.0. This bacterial suspension was immediately used to inoculate electrochemical reactors.

Electrochemical Cell Setup and Biotic Current Measurement: Custom-build single chamber, three electrode electrochemical reactors (Figure S10, Supporting Information) were used for electrochemical testing of *S. oneidensis* on bare ITO, PDA-coated, and PEDOT:PSS/PHEA-coated ITO electrodes. The reactor contained PEDOT:PSS/PHEA-coated ITO working electrode (200.96 mm^2), Ag/AgCl/1 M KCl reference electrode, and a Ti counter electrode. All data in this research were reported versus Ag/AgCl/1 M KCl reference electrode, unless otherwise. Reactors were filled with 16 mL of SBM, held at 30°C , and purged with nitrogen continuously to maintain anaerobic conditions. Chronoamperometric measurements were conducted in triplicate on unmodified and modified ITO electrodes by poisoning the potential of the working electrode at +0.2 V versus Ag/AgCl/1 M KCl reference electrode using a Metrohm DropSens Multi Potentiostat μStat 8000P. *S. oneidensis* were grown overnight in 50 mL SBM, washed with fresh SBM, adjusted to an OD600 of 1.0, and 1 mL of the *S. oneidensis* was inoculated into the electrochemical reactor. The biotic current was continuously measured for 25 h after the inoculation of *S. oneidensis*. The current density was collected every 36 s and the reported data were averaged from triplicate experiments.

Electrochemical Characterization: Cyclic voltammetry (CV) and EIS measurements were conducted using Metrohm DropSens Multi Potentiostat μStat 8000P and BioLogic VMP-300 Potentiostat, respectively. In cyclic voltammetry, the anode was scanned from -0.8 to $+0.4 \text{ V}$ versus Ag/AgCl/1 M KCl reference electrode with a scan rate of 10 mV s^{-1} for three cycles. For EIS measurements, the working electrode was set at $+0.2 \text{ V}$ versus Ag/AgCl, and a potential at $E_{AC} = 5 \text{ mV}$ was used with frequencies ranging from 100 kHz to 100 mHz.

Confocal Laser Scanning Microscopy Characterization: $30 \times 10^{-3} \text{ M}$ SYTO 9 and $30 \times 10^{-3} \text{ M}$ propidium iodide (PI) staining solutions were prepared according to the recommendations from the LIVE/DEAD BacLight bacterial viability kit from ThermoFisher. The reactors were washed twice with fresh SBM prior to staining to remove any unattached microbes. The staining solution containing SYTO 9 and PI was added into the reactors, and the samples were allowed to sit in room temperature for 15 min in dark. The samples were subsequently washed with fresh SBM and held at room temperature in the dark for an additional 15 min. The samples were then chemically fixed with 4% (v/v) glutaraldehyde solution for 30 min. The modified and unmodified ITO electrodes were removed from reactors and allowed to dry for 5 min at room temperature in dark. The stained samples were then covered with mounting oil, masked by #1.5 glass coverslip, and sealed with nail polish. The samples were imaged with 63x and 100x objectives using Zeiss LSM 800. Confocal imaging was conducted using a 488 nm diode laser and 561 nm HeNe laser to excite SYTO 9 and PI, respectively. The bright field images were corrected by shading correction to remove unavoidable stains on the lens. No staining process was required for GFP-expressing *S. oneidensis*. The cell densities were estimated from ImageJ by counting the live and dead cells in a $101.41 \times 101.41 \mu\text{m}^2$ region.

Fourier-Transform Infrared Spectroscopy: The FTIR spectra of all samples were measured by a Thermo Nicolet iS10 FTIR spectrometer using a diamond ATR attachment.

Scanning Electron Microscopy Characterization: After electrochemical testing, microbes on the surfaces of the modified and unmodified electrodes were chemically fixed by immersing the electrodes in 4% (v/v) glutaraldehyde solution for 30 min. Following fixation, a graded series of solution from SBM, DI water, 35% ethanol to 70% ethanol were each changed twice every hour. The electrodes were then immersed in 100% ethanol overnight as the last step of solvent exchange and dried using CO_2 critical point drying (Leica critical point dryer). The electrodes were sputtered with 3 nm of gold before imaging with a FEI Apreo SEM.

Atomic Force Microscopy: AFM measurements were performed with Park AFM NX20 Microscope using a POINTPROBE Silicon SPM sensor. The PEDOT:PSS/PHEA-coated ITO electrodes were scratched by tweezers to create a cut on the electrode allowing the imaging of the thin-film height. The AFM height images were recorded using non-contact mode.

X-ray Photoelectron Spectroscopy: The XPS was conducted on electrodes as prepared. XPS data was obtained by using PHI Quantera XPS.

Time-of-Flight Secondary-Ion Mass Spectrometry: The negative high-mass-resolution depth profile was performed using a TOF-SIMS NCS instrument, which combines a TOF.SIMS.5 instrument (ION-TOF GmbH, Münster, Germany) and an in situ scanning probe microscope (NanoScan, Switzerland) at Shared Equipment Authority from Rice University. A bunched 30 keV Bi_3^+ ions (with a measured current of 0.15 pA) was used as primary probe for analysis (scanned area $100 \times 100 \mu\text{m}^2$), and sputtering was performed using Ar_{1500}^+ ions at 10 keV with a typical current around 0.67 nA, rastered area $500 \times 500 \mu\text{m}^2$. The beams were operated in non-interlaced mode, alternating 1 analysis cycle and 1 sputtering cycle (corresponding to 1.63 s) followed by a pause of 3 s for the charge compensation with an electron flood gun. An adjustment of the charge effects has been operated using a surface potential of 0 V and an extraction bias of -20 V. During the depth profiling, the cycle time was fixed to 200 μs (corresponding to $m/z = 0\text{--}3644$ a.m.u mass range). All depth profiles have been point-to-point normalized by the total ion intensity and the data have been plotted using a 3-points adjacent averaging. Both normalization and smoothing have permitted a better comparison of the data from the different samples. The depth calibrations have been established using the interface tool in SurfaceLab version 7.2 software from ION-TOF GmbH to identify the different interfaces and based on the measured thicknesses using the surface profiler to obtain a line scan of the craters with the in situ SPM by contact scanning.

Microbial Fuel Cell Setup and Power Source Characterization: The preparation of MFC was the same as electrochemical cell setup for biotic current measurement using the same combination of reactors and electrodes. The electrochemical reactors were stabilized overnight purging with nitrogen and microbes were inoculated at the same concentration and same volume. After culturing *S. oneidensis* in the electrochemical reactors for 25 h, electrochemical reactors were connected in series and used to power a 1.8 V red LED light bulb.

Organic Electrochemical Transistor Device Fabrication and Characterization: The source-drain contacts were patterned by covering the glass substrate with polyimide tape and sputtering Cr and Au layers onto the exposed regions with a thickness of 2 and 50 nm. The channel geometry was $100 \mu\text{m} \times 1 \text{ mm}$ (length \times width). The channel was fabricated by spin-coating PEDOT:PSS solution (10% (v/v) EG, 0.25% (v/v) DBSA, 1% (v/v) (3-glycidyloxypropyl)trimethoxysilane (GOPS)) at 1000 rpm for 30 s and was crosslinked at 140°C for 30 min. The PEDOT:PSS solution was filtered by a $0.4 \mu\text{m}$ filter before applying for device fabrication. The biotic samples collected after the chronoamperometric measurement were used as the gate electrode for the OECT performance characterization. OECT devices were characterized using a Yokogawa sourcemeter and experiments were conducted using a customized LabView program. All measurements were examined in fresh SBM with 20 mM of lactate purged with nitrogen. The transfer curves of the OECT device were collected by applying source-drain voltage V_{DS} at -0.6 V while sweeping the gate voltage V_{GS} between -0.8 and 1.2 V. The gate electrodes immobilized with *S. oneidensis* were heated in SBM at 70°C for an hour after the live-cell measurement to inactivate and kill the microbes for dead-cell measurement.

Supporting Information

Supporting Information is available from the Wiley Online Library or from the author.

Acknowledgements

The authors acknowledge support from the National Science Foundation through (CBET-1843556 and NRT-1828869), the Office of Naval Research (N00014-20-1-2274), and the Department of Energy (DE-SC0014462). R.V. and C.-P.T. acknowledge support from the Welch Foundation for Chemical Research (C-1888). ToF-SIMS analysis were carried out with support provided by the National Science Foundation CBET-1626418. This work was conducted in part using resources of the Shared Equipment Authority at Rice University.

Conflict of Interest

The authors declare no conflict of interest.

Data Availability Statement

The data that support the findings of this study are available from the corresponding author upon reasonable request.

Keywords

biosensing, conductive polymers, microbial bioelectronics, microbial fuel cells, organic electrochemical transistors, patterned bioelectronics, poly(3,4-ethylenedioxythiophene)

Received: November 20, 2021

Revised: January 21, 2022

Published online: February 23, 2022

- [1] C.-P. Tseng, J. J. Silberg, G. N. Bennett, R. Verduzco, *ACS Macro Lett.* **2020**, 9, 1590.
- [2] D. R. Bond, D. E. Holmes, L. M. Tender, D. R. Lovley, *Science* **2002**, 295, 483.
- [3] H. Chen, F. Dong, S. D. Minter, *Nat. Catal.* **2020**, 3, 225.
- [4] D. Pant, G. Van Bogaert, L. Diels, K. Vanbroekhoven, *Bioresour. Technol.* **2010**, 101, 1533.
- [5] D. P. Webster, M. A. TerAvest, D. F. R. Doud, A. Chakravorty, E. C. Holmes, C. M. Radens, S. Sureka, J. A. Gralnick, L. T. Angenent, *Biosens. Bioelectron.* **2014**, 62, 320.
- [6] E. A. West, A. Jain, J. A. Gralnick, *ACS Synth. Biol.* **2017**, 6, 1627.
- [7] A. Y. Zhou, M. Baruch, C. M. Ajo-Franklin, M. M. Maharbiz, *PLoS One* **2017**, 12, e0184994.
- [8] J. N. Roy, S. Babanova, K. E. Garcia, J. Cornejo, L. K. Ista, P. Atanasov, *Electrochim. Acta* **2014**, 126, 3.
- [9] M. A. TerAvest, Z. Li, L. T. Angenent, *Energy Environ. Sci.* **2011**, 4, 4907.
- [10] B. E. Logan, M. J. Wallack, K.-Y. Kim, W. He, Y. Feng, P. E. Saikaly, *Environ. Sci. Technol. Lett.* **2015**, 2, 206.
- [11] C. I. Torres, A. K. Marcus, B. E. Rittmann, *Biotechnol. Bioeng.* **2008**, 100, 872.
- [12] J. A. Cornejo, H. Sheng, E. Edri, C. M. Ajo-Franklin, H. Frei, *Nat. Commun.* **2018**, 9, 2263.
- [13] T. Yin, Z. Lin, L. Su, C. Yuan, D. Fu, *ACS Appl. Mater. Interfaces* **2015**, 7, 400.
- [14] K. Yagi, *Appl. Microbiol. Biotechnol.* **2007**, 73, 1251.
- [15] C. Li, S. Cheng, *Crit. Rev. Biotechnol.* **2019**, 39, 1015.
- [16] D. F. Williams, *Biomaterials* **2014**, 35, 10009.
- [17] C. Santoro, C. Arbizzani, B. Erable, I. Ieropoulos, *J. Power Sources* **2017**, 356, 225.

- [18] X. Xie, C. Criddle, Y. Cui, *Energy Environ. Sci.* **2015**, *8*, 3418.
- [19] R.-B. Song, Y. Wu, Z.-Q. Lin, J. Xie, C. H. Tan, J. S. C. Loo, B. Cao, J.-R. Zhang, J.-J. Zhu, Q. Zhang, *Angew. Chem., Int. Ed.* **2017**, *56*, 10516.
- [20] T. J. Zajdel, M. Baruch, G. Méhes, E. Stavrinidou, M. Berggren, M. M. Maharbiz, D. T. Simon, C. M. Ajo-Franklin, *Sci. Rep.* **2018**, *8*, 15293.
- [21] E. Kipf, J. Koch, B. Geiger, J. Erben, K. Richter, J. Gescher, R. Zengerle, S. Kerzenmacher, *Bioresour. Technol.* **2013**, *146*, 386.
- [22] X. Fang, S. Kalathil, G. Divitini, Q. Wang, E. Reisner, *Proc. Natl. Acad. Sci. USA* **2020**, *117*, 5074.
- [23] B. Li, B. E. Logan, *Colloids Surf., B* **2004**, *36*, 81.
- [24] K. Guo, B. C. Donose, A. H. Soeriyadi, A. PrévotEAU, S. A. Patil, S. Freguia, J. J. Gooding, K. Rabaey, *Environ. Sci. Technol.* **2014**, *48*, 7151.
- [25] X. Liu, W. Wu, Z. Gu, *J. Power Sources* **2015**, *277*, 110.
- [26] S. Wu, E. Kim, J. Li, W. E. Bentley, X.-W. Shi, G. F. Payne, *ACS Appl. Electron. Mater.* **2019**, *1*, 1337.
- [27] E. Kim, T. Gordonov, W. E. Bentley, G. F. Payne, *Anal. Chem.* **2013**, *85*, 2102.
- [28] R. Kaur, A. Marwaha, V. A. Chhabra, K.-H. Kim, S. K. Tripathi, *Renewable Sustainable Energy Rev.* **2020**, *119*, 109551.
- [29] Y. Hindatu, M. S. M. Annuar, A. M. Gumel, *Renewable Sustainable Energy Rev.* **2017**, *73*, 236.
- [30] K. Guo, A. PrévotEAU, S. A. Patil, K. Rabaey, *Curr. Opin. Biotechnol.* **2015**, *33*, 149.
- [31] G. G. kumar, V. G. S. Sarathi, K. S. Nahm, *Biosens. Bioelectron.* **2013**, *43*, 461.
- [32] H. Ren, H. Tian, C. L. Gardner, T.-L. Ren, J. Chae, *Nanoscale* **2016**, *8*, 3539.
- [33] B. Piro, G. Mattana, S. Zrig, G. Anquetin, N. Battaglini, D. Capitao, A. Maurin, S. Reisberg, *Appl. Sci.* **2018**, *8*, 928.
- [34] D. Mantione, I. del Agua, A. Sanchez-Sanchez, D. Mecerreyes, *Polymers* **2017**, *9*, 354.
- [35] K. Sun, S. Zhang, P. Li, Y. Xia, X. Zhang, D. Du, F. H. Isikgor, J. Ouyang, *J. Mater. Sci.: Mater. Electron.* **2015**, *26*, 4438.
- [36] L. Han, K. Liu, M. Wang, K. Wang, L. Fang, H. Chen, J. Zhou, X. Lu, *Adv. Funct. Mater.* **2018**, *28*, 1704195.
- [37] R. A. Green, R. T. Hassarati, L. Bouchinet, C. S. Lee, G. L. M. Cheong, J. F. Yu, C. W. Dodds, G. J. Suening, L. A. Poole-Warren, N. H. Lovell, *Biomaterials* **2012**, *33*, 5875.
- [38] Z. Mekhalif, P. Lang, F. Garnier, *J. Electroanal. Chem.* **1995**, *399*, 61.
- [39] C. Boehler, F. Oberueber, S. Schlabach, T. Stieglitz, M. Asplund, *ACS Appl. Mater. Interfaces* **2017**, *9*, 189.
- [40] Y.-T. Tseng, Y.-C. Lin, C.-C. Shih, H.-C. Hsieh, W.-Y. Lee, Y.-C. Chiu, W.-C. Chen, *J. Mater. Chem. C* **2020**, *8*, 6013.
- [41] B. D. Paulsen, R. Wu, C. J. Takacs, H.-G. Steinrück, J. Strzalka, Q. Zhang, M. F. Toney, J. Rivnay, *Adv. Mater.* **2020**, *32*, 2003404.
- [42] G. Rebetez, O. Bardagot, J. Affolter, J. Réhault, N. Banerji, *Adv. Funct. Mater.* **2021**, *32*, 2105821.
- [43] S. R. McCuskey, Y. Su, D. Leifert, A. S. Moreland, G. C. Bazan, *Adv. Mater.* **2020**, *32*, 1908178.
- [44] Y. Yuan, S. Zhou, N. Xu, L. Zhuang, *Appl. Microbiol. Biotechnol.* **2011**, *89*, 1629.
- [45] D. Hidalgo, A. Sacco, S. Hernández, T. Tommasi, *Bioresour. Technol.* **2015**, *195*, 139.
- [46] P. V. Sarma, C. S. Tiwary, S. Radhakrishnan, P. M. Ajayan, M. M. Shaijumon, *Nanoscale* **2018**, *10*, 9516.
- [47] J. Song, Y. Li, F. Yin, Z. Zhang, D. Ke, D. Wang, Q. Yuan, X.-E. Zhang, *ACS Sens.* **2020**, *5*, 1795.
- [48] L. Shi, H. Dong, G. Reguera, H. Beyenal, A. Lu, J. Liu, H.-Q. Yu, J. K. Fredrickson, *Nat. Rev. Microbiol.* **2016**, *14*, 651.
- [49] E. Mevers, L. Su, G. Pishchany, M. Baruch, J. Cornejo, E. Hobert, E. Dimise, C. M. Ajo-Franklin, J. Clardy, *eLife* **2019**, *8*, e48054.
- [50] S. Xu, Y. Jiang, M. Y. El-Naggar, *Electrochim. Acta* **2016**, *198*, 49.
- [51] E. Marsili, D. B. Baron, I. D. Shikhare, D. Coursolle, J. A. Gralnick, D. R. Bond, *Proc. Natl. Acad. Sci. USA* **2008**, *105*, 3968.
- [52] Y. Hu, Y. Yang, E. Katz, H. Song, *Chem. Commun.* **2015**, *51*, 4184.
- [53] B. E. Logan, *Nat. Rev. Microbiol.* **2009**, *7*, 375.
- [54] I. Schmidt, A. Gad, G. Scholz, H. Boht, M. Martens, M. Schilling, H. S. Wasisto, A. Waag, U. Schröder, *Biosens. Bioelectron.* **2017**, *94*, 74.
- [55] D. Q. Le, S. Tokonami, T. Nishino, H. Shiigi, T. Nagaoka, *Bioelectrochemistry* **2015**, *105*, 50.
- [56] B. Cao, Z. Zhao, L. Peng, H.-Y. Shiu, M. Ding, F. Song, X. Guan, C. K. Lee, J. Huang, D. Zhu, X. Fu, G. C. L. Wong, C. Liu, K. Neelson, P. S. Weiss, X. Duan, Y. Huang, *Science* **2021**, *373*, 1336.
- [57] L. Peng, S.-J. You, J.-Y. Wang, *Biosens. Bioelectron.* **2010**, *25*, 1248.
- [58] R. Nakamura, F. Kai, A. Okamoto, G. J. Newton, K. Hashimoto, *Angew. Chem.* **2009**, *121*, 516.
- [59] A. Deeke, T. H. J. A. Sleutels, H. V. M. Hamelers, C. J. N. Buisman, *Environ. Sci. Technol.* **2012**, *46*, 3554.
- [60] X. Xie, L. Hu, M. Pasta, G. F. Wells, D. Kong, C. S. Criddle, Y. Cui, *Nano Lett.* **2011**, *11*, 291.
- [61] X.-W. Liu, X.-F. Sun, Y.-X. Huang, G.-P. Sheng, S.-G. Wang, H.-Q. Yu, *Energy Environ. Sci.* **2011**, *4*, 1422.
- [62] Y.-C. Yong, Y.-Y. Yu, X. Zhang, H. Song, *Angew. Chem., Int. Ed.* **2014**, *53*, 4480.
- [63] Y.-C. Yong, X.-C. Dong, M. B. Chan-Park, H. Song, P. Chen, *ACS Nano* **2012**, *6*, 2394.
- [64] M. Chen, X. Zhou, X. Liu, R. J. Zeng, F. Zhang, J. Ye, S. Zhou, *Biosens. Bioelectron.* **2018**, *108*, 20.
- [65] L. Ren, S. R. McCuskey, A. Moreland, G. C. Bazan, T.-Q. Nguyen, *Biosens. Bioelectron.* **2019**, *144*, 111630.
- [66] Y. Tao, Q. Liu, J. Chen, B. Wang, Y. Wang, K. Liu, M. Li, H. Jiang, Z. Lu, D. Wang, *Environ. Sci. Technol.* **2016**, *50*, 7889.
- [67] R. Starwalt-Lee, M. Y. El-Naggar, D. R. Bond, J. A. Gralnick, *Mol. Microbiol.* **2021**, *115*, 1069.
- [68] M. A. TerAvest, C. M. Ajo-Franklin, *Biotechnol. Bioeng.* **2016**, *113*, 687.
- [69] H. W. Harris, M. Y. El-Naggar, O. Bretschger, M. J. Ward, M. F. Romine, A. Y. Obraztsova, K. H. Neelson, *Proc. Natl. Acad. Sci. USA* **2010**, *107*, 326.
- [70] A. Y. Chen, Z. Deng, A. N. Billings, U. O. S. Seker, M. Y. Lu, R. J. Citorik, B. Zakeri, T. K. Lu, *Nat. Mater.* **2014**, *13*, 515.
- [71] Y. Cao, Y. Feng, M. D. Ryser, K. Zhu, G. Herschlag, C. Cao, K. Marusak, S. Zauscher, L. You, *Nat. Biotechnol.* **2017**, *35*, 1087.
- [72] M. Lienemann, M. A. TerAvest, J.-P. Pitkänen, I. Stuns, M. Penttilä, C. M. Ajo-Franklin, J. Jäntti, *Microb. Biotechnol.* **2018**, *11*, 1184.
- [73] J. Rivnay, S. Inal, A. Salleo, R. M. Owens, M. Berggren, G. G. Malliaras, *Nat. Rev. Mater.* **2018**, *3*, 17086.
- [74] G. Méhes, A. Roy, X. Strakosas, M. Berggren, E. Stavrinidou, D. T. Simon, *Adv. Sci.* **2020**, *7*, 2000641.
- [75] J. T. Atkinson, L. Su, X. Zhang, G. N. Bennett, J. J. Silberg, C. M. Ajo-Franklin, *bioRxiv* **2021**, <https://doi.org/10.1101/2021.06.04.447163>.
- [76] H. Lee, S. M. Dellatore, W. M. Miller, P. B. Messersmith, *Science* **2007**, *318*, 426.
- [77] M. S. Waters, C. A. Sturm, M. Y. El-Naggar, A. Luttge, F. E. Udawadia, D. G. Cvitkovitch, S. D. Goodman, K. H. Neelson, *Geobiology* **2008**, *6*, 254.
- [78] D. Baron, E. LaBelle, D. Coursolle, J. A. Gralnick, D. R. Bond, *J. Biol. Chem.* **2009**, *284*, 28865.